STEM CELLS AND DEVELOPMENT
Volume 23, Number 18, 2014

DOI: 10.1089/scd.2013.0344

Comparative Analysis of Mouse-Induced Pluripotent Stem Cells and Mesenchymal Stem Cells During Osteogenic Differentiation In Vitro

Hiroshi Egusa,[1,2] Hiroki Kayashima,[1] Jiro Miura,[3] Shinya Uraguchi,[1] Fangfang Wang,[1] Hiroko Okawa,[1] Jun-Ichi Sasaki,[1] Makio Saeki,[4] Takuya Matsumoto,[5] and Hirofumi Yatani[1]

Induced pluripotent stem cells (iPSCs) can differentiate into mineralizing cells and are, therefore, expected to be useful for bone regenerative medicine; however, the characteristics of iPSC-derived osteogenic cells remain unclear. Here, we provide a direct in vitro comparison of the osteogenic differentiation process in mesenchymal stem cells (MSCs) and iPSCs from adult C57BL/6J mice. After 30 days of culture in osteogenic medium, both MSCs and iPSCs produced robustly mineralized bone nodules that contained abundant calcium phosphate with hydroxyapatite crystal formation. Mineral deposition was significantly higher in iPSC cultures than in MSC cultures. Scanning electron microscopy revealed budding matrix vesicles in early osteogenic iPSCs; subsequently, the vesicles propagated to exhibit robust mineralization without rich fibrous structures. Early osteogenic MSCs showed deposition of many matrix vesicles in abundant collagen fibrils that became solid mineralized structures. Both cell types demonstrated increased expression of osteogenic marker genes, such as *runx2*, osterix, *dlx5*, bone sialoprotein (BSP), and osteocalcin, during osteogenesis; however, real-time reverse transcription–polymerase chain reaction array analysis revealed that osteogenesis-related genes encoding mineralization-associated molecules, bone morphogenetic proteins, and extracellular matrix collagens were differentially expressed between iPSCs and MSCs. These data suggest that iPSCs are capable of differentiation into mature osteoblasts whose associated hydroxyapatite has a crystal structure similar to that of MSC-associated hydroxyapatite; however, the transcriptional differences between iPSCs and MSCs could result in differences in the mineral and matrix environments of the bone nodules. Determining the biological mechanisms underlying cell-specific differences in mineralization during in vitro iPSC osteogenesis may facilitate the development of clinically effective engineered bone.

Introduction

As populations in developed countries age, the prevalence of musculoskeletal disorders will continue to increase [1]. Orthopedic surgical procedures for the musculoskeletal system require the regular use of bone grafts that facilitate timely healing of injuries [2]. In dentistry, the recent increase in the demand for dental implants has generated a need for robust bone augmentation in the atrophic alveolar ridge and the maxillary sinus [3,4]. At present, autologous bone is the standard for bone grafting; however, limited tissue supply makes large defects problematic to repair, and this approach is also associated with a risk of donor-site morbidity. These disadvantages have resulted in the proposal of novel treatments and encouraged the development of stem-cell-based tissue engineering therapy as an alternative method.

Recently, many studies have demonstrated potential advantages for stem-cell-based therapies in regenerative treatments. Adult mesenchymal stem cells (MSC) are now an excellent candidate for tissue replacement therapies, and tissue engineering approaches using autologous MSCs represent the clinical state of the art for stem-cell-based bone regeneration [4,5]. However, it is still challenging

[1]Division of Oromaxillofacial Regeneration, Department of Fixed Prosthodontics, Osaka University Graduate School of Dentistry, Suita, Osaka, Japan.
[2]Division of Molecular and Regenerative Prosthodontics, Tohoku University Graduate School of Dentistry, Sendai, Miyagi, Japan.
[3]Division for Interdisciplinary Dentistry, Osaka University Dental Hospital, Suita, Osaka, Japan.
[4]Division of Dental Pharmacology, Niigata University Graduate School of Medical and Dental Sciences, Niigata, Japan.
[5]Department of Biomaterials, Graduate School of Medicine, Dentistry and Pharmaceutical Sciences, Okayama University, Okayama, Japan.

to amplify isolated MSCs in sufficient quantities to provide clinical efficacy. Recently, induced pluripotent stem cells (iPSCs) [6,7] have received attention in regenerative medicine because of their unlimited self-renewal capacity and embryonic stem cell (ESC)-like developmental plasticity [8]. iPSCs have great potential for personalized regenerative cell therapies, because they can be generated artificially via genetic manipulation from any type of patient-derived somatic cell. In addition, iPSCs make it possible to avoid the ethical issues surrounding the use of ESCs and problems with rejection after the implantation of nonautologous cells.

If iPSCs are to be considered for the development of tissue-engineered bone substitutes, a comprehensive understanding of their differentiation process is necessary. To date, the differentiation mechanisms of MSCs have been well studied, and methods that guide MSC differentiation into mature osteoblasts using osteogenic induction factors, such as dexamethasone, ascorbic acid, and β-glycerophosphate, have been well established [9]. Using these classical osteogenic induction factors, several studies have examined the in vitro-directed mineralization capacity [10–14] and in vivo bone formation potential [15,16] of mouse iPSCs. In these studies, the in vitro calcification potential of iPSCs was evaluated using a combination of osteogenic molecular markers, gene expression, and histological staining [10–16], but no study to date has assessed the structural properties or elemental composition of the mineralized extracellular matrix (ECM). It is often difficult to determine whether osteogenically induced cells, indeed, produce bonelike calcium phosphate mineral similar to native osteoblasts, especially when using osteogenic marker gene expression and histological staining techniques, such as the von Kossa and Alizarin Red methods [17]. Therefore, other techniques such as electron microscopy, X-ray diffraction, and Fourier transform infrared spectroscopy (FTIR) are recommended to verify the presence and quality of calcium phosphate phases [17]. However, it is still uncertain whether iPSCs can differentiate into mature osteoblasts and produce mineralized ECM components similar to those produced by MSCs.

This question prompted us to perform a direct comparison of these cell sources from the same mouse strain with regard to osteogenic characteristics by using the methods of electron microscopic analysis, X-ray diffraction, and FTIR in addition to comprehensive osteogenic gene expression analysis. The objective of this study was to investigate whether a classical osteogenic induction method for MSCs also guides iPSC differentiation into mature osteoblasts through the same ECM mineralization process used by MSCs.

Materials and Methods

Cell cultures

Both clonal iPSCs and MSCs were established from 10-week-old adult male C57BL/6J mice according to protocols approved by the Institutional Animal Care and Use Committee of Osaka University Graduate School of Dentistry (approval No. 19-054-1 and 20-009-1). The mouse iPSCs used in this study were gingival fibroblast-derived iPSCs that had been previously generated [18] using retroviral introduction of Oct3/4, Sox2, and Klf4. This iPSC clone (clone mGF-iPS-3F-3) presented germline transmission, which is proof that the generated iPSCs were of high quality [18]. The clonal MSCs (mBMSC-4), which we established from mouse femur bone marrow, were multipotent, as demonstrated by their ability to differentiate specifically into osteoblast, adipocyte, chondrocyte, and myoblast lineages [19,20].

iPSCs were maintained on SNLP76.7-4 feeder cells in ''ES medium,'' which consisted of Dulbecco's modified Eagle's medium (DMEM with 4.5 g/L glucose and without sodium pyruvate; Nacalai Tesque), 15% fetal bovine serum (FBS), 2 mM L-glutamine, 1×10^{-4} M nonessential amino acids, 1×10^{-4} M 2-mercaptoethanol, 50 U of penicillin, and 50 μg/mL streptomycin [18]. MSCs were maintained in ''MSC medium'' consisting of minimum essential medium Eagle, alpha modification (α-MEM; Nacalai Tesque) supplemented with 15% FBS, 100 U/mL penicillin, 100 μg/mL streptomycin, and 250 ng/mL amphotericin B [21].

Osteogenic induction

Before osteogenic induction, iPSCs were cultured as floating embryoid bodies (EBs) [22] in the presence of all-trans retinoic acid (RA; Sigma) to guide differentiation into immature mesenchymal cells [23]. Briefly, iPSCs were harvested by trypsinization (0.25% trypsin and 1 mM EDTA) and transferred to low-attachment bacterial culture dishes (Sterilin®; Thermo Fisher Scientific) in the ES medium to form EBs (Fig. 1A). After 2 days, floating EBs were collected by centrifugation (300 rpm for 2 min), and they were maintained in ES medium that was supplemented with 1 μM RA for another 2 days on low-attachment culture dishes. Then, the EBs were collected and aliquoted suspensions were prepared. To calculate the cell seeding density, one of the aliquots was subjected to cell counting by a cell counter (Z1D Coulter Counter®; Beckman Coulter) after dissociation of the EBs to single cells by treatment with 0.25% trypsin/1 mM EDTA. The obtained concentration of dissociated cells was used to calculate the seeding volume for the other aliquots of suspended EBs. The suspended EBs were plated onto 0.1% gelatin-coated six-well cell culture plates (7.3×10^4 cells/cm^2) in ES medium with 1 μM RA, followed by 1-day culture until osteogenic induction commenced. MSCs were plated on 0.1% gelatin-coated six-well cell culture plates (7.3×10^4 cells/cm^2) in MSC medium 1 day before osteogenic induction.

For osteogenic induction, the culture medium of iPSCs and MSCs was replaced with osteogenic induction medium [21] consisting of α-MEM that was supplemented with 15% FBS, 0.1 μM dexamethasone, 10 mM β-glycerophosphate, 50 μM ascorbate-2-phosphate, 100 U/mL penicillin, 100 μg/mL streptomycin, and 250 ng/mL amphotericin B. ES medium and MSC medium were used in control cultures for iPSCs and MSCs, respectively. Each culture medium was changed every 2–3 days, and cultures were maintained for 30 days. Day 0 refers to the day when the osteogenic induction commenced.

von Kossa staining

Cells were fixed in 10% formalin neutral buffer solution (Wako) for von Kossa staining. Nodule mineralization was visualized by treatment with 5% silver nitrate (Sigma) solution under ultraviolet light for 30 min, followed by 5% sodium thiosulfate (Sigma) solution for 5 min [24].

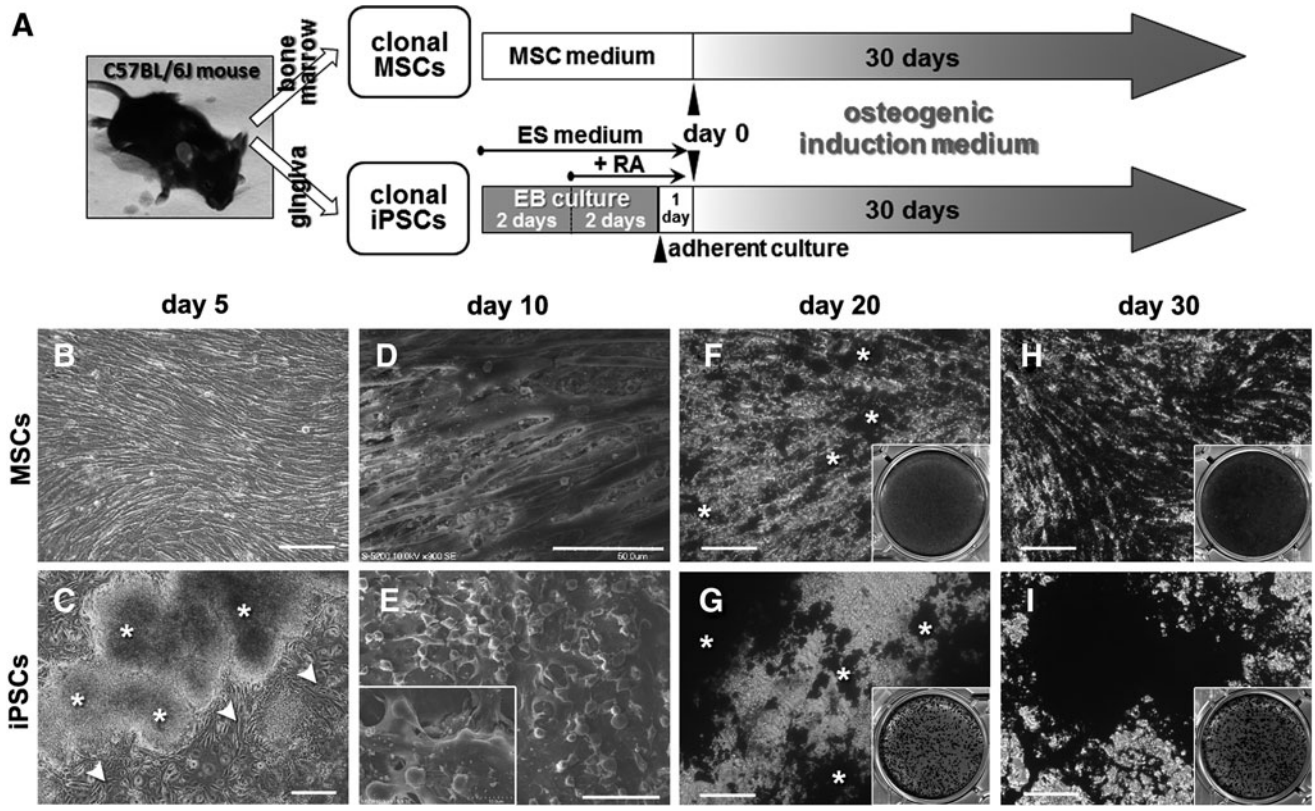

FIG. 1. Osteogenic induction of mesenchymal stem cells (MSCs) and induced pluripotent stem cells (iPSCs). **(A)** Cell culture and osteogenic induction methods for MSCs and iPSCs. Clonal MSCs and iPSCs were established from the C57BL/6J mouse strain using bone marrow and gingival tissues, respectively. ''MSC medium'' and ''ES medium'' are growth media for MSCs and iPSCs, respectively. ''EB culture'' represents floating culture of iPSCs forming embryoid bodies. RA, all-trans retinoic acid. ''Day 0'' refers to the day when osteogenic induction commences. The ''osteogenic induction medium'' contained the osteogenic factors dexamethasone, β-glycerophosphate, and ascorbate-2-phosphate. **(B-I)** MSC and iPSC cultures during osteogenic induction. **(B, C)** Phase-contrast photomicrographs on day 5 (scale bars: 100 μm). **(B)** MSC culture showed elongated fibroblastic cells in confluence. **(C)** iPSC culture showed fibroblastic cells (*arrowheads*) that migrated from the attached EBs (*asterisks*). **(D, E)** Scanning electron microscopic images on day 10 (scale bars: 50 μm). **(D)** MSC culture showed elongated spindle-like cells in monolayer. **(E)** iPSC culture showed multilayer cells and many rounded cells on the surface of the layers. **(F–I)** von Kossa staining images on day 20 **(F, G)** and 30 **(H, I)** (scale bars: 100 μm). **(F, H)** MSC culture on day 20 exhibited a von Kossa-positive area (*asterisks*) **(F)**, which evenly spread over the cell culture on day 30 **(H). (G, I)** iPSC culture on day 20 exhibited studded von Kossa-positive areas (*asterisks*) concentrated on and around cell aggregates **(G)**, which are more apparent on day 30 **(I)**. *Insets*: von Kossa staining results in six-well culture plates.

Calcium measurement

To measure calcium deposition, cells in six-well culture plates were washed with phosphate-buffered saline (PBS), decalcified with 3 mL of 5 M acetic acid, and then maintained overnight at room temperature. Insoluble components were removed by centrifugation (2,300 *g* for 10 min). The calcium concentrations in the supernatants were then determined by a colorimetric method (OD: 595 nm) using a commercial kit (Calcium E-Test kit; Wako). The calcium deposition per well of each cell culture was then calculated.

Scanning electron microscopy and energy-dispersive X-ray spectroscopy

Energy-dispersive X-ray spectroscopy (EDX) analysis was applied to characterize the minerals in the cell specimens. Cells were fixed with 10% formalin neutral buffer solution. Cell specimens were washed with PBS and dehydrated in a series of ethanol concentrations of approximately 100%. The specimens were dried by a critical-point dryer (HCP-2; Hitachi) with CO_2 and then coated with osmium to a thickness of 5 nm. Samples were analyzed using a field-emission scanning electron microscope (FE-SEM, S-5200; Hitachi) with an energy-dispersive X-ray spectrometry analyzer (Genesis; EDAX) at an accelerating voltage of 20 kV [25].

FTIR analysis

FTIR analysis was conducted to investigate the elemental composition of the mineralized ECM of the cell samples. Cells were fixed in 10% formalin neutral buffer solution and washed with distilled water, followed by dehydration in a series of ethanol concentrations of up to 100%. The specimens were dried in a dry-heat sterilizer at 37°C for 12 h. The powdered samples were mixed with powdered potassium

bromide (Sigma) at a concentration of 2% (w/v) [26]. The FTIR spectra for the diffuse reflectance of the powdered samples were recorded on an FTIR-8300 spectrophotometer (Shimadzu). The data for 50 scans in the range of 700–1,900 cm^{-1} at a resolution of 1 cm^{-1} were collected and averaged.

Transmission electron microscopy and selected area electron diffraction analysis

Cells were fixed with 2% paraformaldehyde and 2.5% glutaraldehyde in 0.1 M sodium cacodylate buffer and then dehydrated in an ascending series of ethanol. Cell specimens were embedded in epoxy resin (Quetol812; Nisshin EM). After curing, samples were sectioned to a thickness of 100 nm with a diamond knife and mounted on copper grids (Nisshin EM) in an ultramicrotome (Ultrotome V; LKB). Some ultra-thin sections were stained with 1% uranium acetate and 0.4% lead citrate [27] for transmission electron microscopy (TEM, H800; Hitachi), whereas other sections without staining were used for selected area electron diffraction (SAED) analysis at 200 kV to determine the presence of hydroxyapatite structure in the mineralized ECM of the cell specimen [28,29].

Real-time reverse transcription–polymerase chain reaction analysis

Total RNA was isolated using an RNeasy Mini Kit (Qiagen). After DNase I treatment (Ambion), cDNA was synthesized from 1 μg of total RNA using oligo dT primers (Promega) and Super Script III reverse transcriptase (Invitrogen). A quantitative TaqMan® real-time reverse transcription-polymerase chain reaction (RT-PCR) analysis for the expression of osterix, bone sialoprotein (BSP), and *osteocalcin* was performed using an ABI 7300 real-time PCR system (Applied Biosystems). Expression of glyceraldehyde-3-phosphate dehydrogenase (*GAPDH*) mRNA was used as an internal control. The TaqMan primer and probe sets used were Mm00504574_m1 (osterix), Mm00492555_m1 (BSP), Mm03413826_mH (osteocalcin), and 4352339E (*GAPDH*).

The levels of *runx2* and *dlx5* mRNA transcripts relative to the level of *GAPDH* transcripts as a control were determined by quantitative RT-PCR using Thunderbird™ SYBR® qPCR Mix (Toyobo) and specific primers (Table 1) on the ABI 7300 real-time PCR system. Primer sets (0.3 μM final concentration for each primer) were used in a final volume of 25 μL per tube. The thermal profile of the PCR was 95°C for 10 min, followed by 40 cycles at 95°C for 15 s and 60°C for 1 min. For confirmation of primer specificity, amplicon length was verified by electrophoresis of products through a 2% agarose gel. The comparative C_T ($2^{-\Delta\Delta CT}$) method [30] was used to evaluate fold gene expression differences between samples.

Real-time RT-PCR array analysis

The mRNA of iPSCs or MSCs was converted into cDNA using the RT^2 First-Strand Kit (Qiagen). The cDNA was then added to the RT^2 SYBR® Green qPCR Master Mix (Qiagen), and each sample was aliquotted on a Mouse Osteogenesis RT^2 Profiler™ PCR Array (Qiagen) to monitor the expression of 84 genes related to osteogenic differentiation (Supplementary Table S1; Supplementary Data are available online at www.liebertpub.com/scd) and five housekeeping genes. All steps were performed according to the manufacturer's protocols for the RT^2 Profiler PCR Array and the ABI 7300 real-time PCR system. Scatter plotting analysis was performed for the PCR array data using the software (RT^2 Profiler PCR Array Data Analysis Version 3.5) on the manufacturer's website (http://pcrdataanalysis.sabiosciences.com/). Data normalization was automatically performed by the software by correcting all Ct values with regard to the Ct values of the available housekeeping genes on the PCR array. A cutoff Ct value of 35 was applied for the analysis in accordance with the manufacturer's recommendations.

Statistical analyses

A one-way analysis of variance (ANOVA) with Tukey or Dunnett post hoc tests was used for comparisons of more than two groups. A significant difference was defined when $P < 0.05$.

Results

ECM mineralization of MSCs and iPSCs

MSCs in osteogenic induction medium adhered to gelatin-coated plates and reached confluence around day 5 (Fig. 1B). EBs of iPSCs in ES medium adhered to gelatin-coated plates within 24 h. When the medium was changed into osteogenic induction medium (day 0), fibroblastic cells dominantly migrated out of the EBs and reached confluence around day 5 (Fig. 1C). SEM on day 10 revealed an apparent morphological difference between MSCs and iPSCs: MSCs spread with an elongated spindle-like morphology almost in a monolayer flat on the surface of the culture dish (Fig. 1D),

Table 1. Primers Used for SYBR® Green Real-Time Reverse Transcription–Polymerase Chain Reaction

Gene	*Primers*	*Product size (bp)*	*Reference sequence*[a]
runx2	Fw: 5′-CGG GCT ACC TGC CAT CAC-3′ Rv: 5′-GGC CAG AGG CAG AAG TCA GA-3′	78	NM_001145920.1
dlx5	Fw: 5′-GCC CCT ACC ACC AGT ACG-3′ Rv: 5′-TCA CCA TCC TCA CCT CTG-3′	96	NM_010056.2
GAPDH	Fw: 5′-TGC ACC ACC AAC TGC TTA G-3′ Rv: 5′-GGA TGC AGG GAT GAT GTT C-3′	117	NM_008084.2

[a]GeneBank accession number.
Fw, forward; Rv, reverse.

whereas iPSCs had multiple layers, and many small rounded cells grew on the fibroblastic cell layers (Fig. 1E). After 20 days of induction, both cell types clearly formed dense structures described in the literature as ''bone nodules'' [31,32]. The nodules on day 20 showed positive von Kossa staining, presenting as black areas in both cell cultures (Fig. 1F, G). Mineralized nodule formation became more apparent on day 30 in both cell types (Fig. 1H, I); however, the distribution of the mineralized nodules appeared different on visual inspection. The von Kossa-positive area in MSC cultures was almost evenly spread over the monolayer of cells (Fig. 1F, H), whereas von Kossa staining in iPSCs was studded and concentrated in an area with dense cell aggregation (Fig. 1G, I).

Differentiation of MSCs and iPSCs in osteogenic medium into mature osteoblasts was further evaluated by calcium deposition and FTIR analysis. Both MSCs and iPSCs showed increased calcium deposition from day 20 to 30 (Fig. 2A). The calcium deposition per well for iPSCs in osteogenic medium was significantly higher than that for MSCs on days 20 and 30. In the FTIR analysis, infrared absorption peaks associated with major bone-related molecular species, such as phosphate, carbon, and amino acids, appeared in the osteogenic MSC and iPSC cultures and increased over time (Fig. 2B). After 30 days of osteogenic induction, the infrared spectra of both the MSCs and iPSCs became similar to the typical infrared spectra of bone [33], showing distinct absorbance bands for vibrations of phosphate, carbonate, and amide I and II.

SEM observation and elemental analysis of MSCs and iPSCs during osteogenesis

SEM images of osteogenically induced MSCs showed long spindle-shaped cells on day 10 that displayed numerous intercellular cytoplasmic processes (Fig. 3A). The gaps of the cellular processes were connected by fibrous structures and punctate small globular vesicle structures (Fig. 3B). EDX analysis demonstrated that elemental calcium and phosphorous were distributed mainly on the vesicle structures in the ECM spaces and on the cell surfaces (Fig. 3C). On day 30 in osteogenic induction medium, MSCs were widened and relatively amorphous (Fig. 3D), and the fibrous and globular components were almost embedded within the solid structure (Fig. 3E). The EDX spectrum displayed high peaks corresponding to elemental phosphorous and calcium that existed on the surface of the tissue (Fig. 3F). In contrast, MSCs cultured for 30 days in growth medium maintained their long spindle shape (Supplementary Fig. S1A), and the ECM space was filled with fibrous structures (Supplementary Fig. S1B). EDX analysis did not show distinct peaks for elemental phosphorous and calcium (Supplementary Fig. S1C).

SEM images of iPSCs on day 10 in osteogenic induction medium revealed that many rounded cells with small globular vesicles were present among the fibroblastic cells, which were multilayered (Fig. 4A). The surface of the rounded cells was covered with many tiny microvillus-like projections (Fig. 4B), and it should be noted that small amorphous vesicles budded from the plasma membrane of the rounded cells. The EDX spectrum displayed small peaks corresponding to phosphorous and calcium, which were distributed on the cell surface but did not specifically accumulate in the vesicular accretions (Fig. 4C). On day 30 in osteogenic induction medium, the rounded iPSCs were covered by small granulated accretions (Fig. 4D), which appeared to be ruptured vesicles (Fig. 4E). The EDX spectrum displayed high peaks corresponding to elemental phosphorous and calcium present in the accretions covering the rounded cells (Fig. 4F). In contrast, iPSCs cultured for 30 days in growth medium contained many flat cells and rounded cells that did not have vesicular accretions (Supplementary Fig. S1D, S1E). EDX

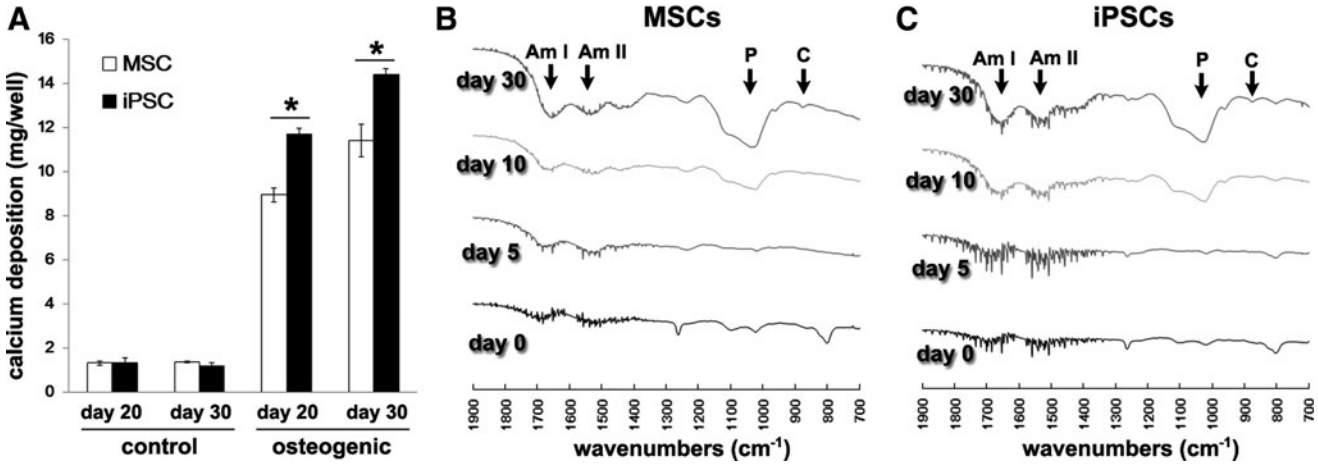

FIG. 2. Mineralization of bone-like extracellular matrix (ECM) in MSCs and iPSCs. **(A)** Calcium deposition per well of MSC and iPSC cultures in control medium (control) or osteogenic induction medium (osteogenic) on days 20 and 30 was evaluated by the calcium measurement assay. The data represent the mean values ± SD of triplicate samples [$*P < 0.001$: analysis of variance (ANOVA) with Tukey's multiple-comparison test]. Fourier transform infrared spectroscopy (FTIR) spectra of MSCs **(B)** and iPSCs **(C)** during osteogenic induction. After 30 days of osteogenic induction, both MSCs and iPSCs exhibited bands of a similar absorbance for vibrations of phosphate (P: association with the mineral hydroxyapatite), carbonate (C: association with carbonate substitution for hydroxyl and phosphate groups in hydroxyapatite) and amide I (Am I), and II (Am II) (association with the protein constituents of bone). It should be noted that these absorption peaks are not evident on days 0 and 5 of induction.

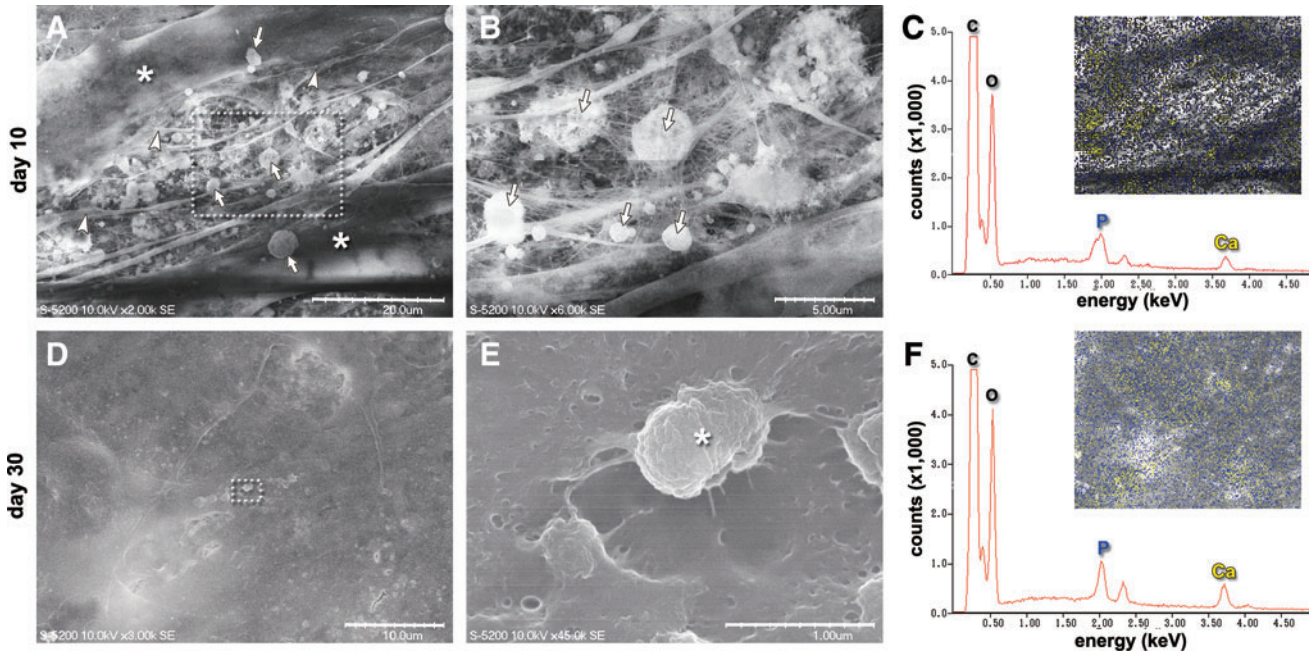

FIG. 3. Scanning electron microscopy (SEM) observation of MSCs during osteogenic differentiation. **(A–C)** Day 10. **(A)** Many cytoplasmic processes (*arrowheads*) and punctate globular vesicle structures (*arrows*) were observed in the extracellular spaces of long spindle-shaped MSCs (*asterisks*). Scale bar: 20 μm. **(B)** Magnification of the *dotted square* in **(A)**. The globular vesicles (*arrows*) were intertwined with collagen fibrils. Scale bar: 5 μm. **(D–F)** Day 30. **(D)** MSCs showed a planar and solid structure. Scale bar: 10 μm. **(E)** Magnification of the *dotted square* in **(D)**. Fibrous and vesicle structures were rarely observed. The remaining vesicle (*asterisk*) was almost embedded within the solid structure. Scale bar: 1 μm. **(C, F)** energy-dispersive X-ray spectroscopy (EDX) analyses of the areas shown in SEM images **(A)** and **(D)**, respectively. Energy peaks in the EDX graph correspond to elemental phosphorous (P), calcium (Ca), carbon (C), and oxygen (O). *Insets*: The *yellow* and *blue dots* represent the elemental distribution of calcium and phosphorous, respectively. **(C)** Elemental calcium and phosphorous accumulated in the fibril and vesicle structures in the intracellular spaces by day 10. **(F)** The surface of the solid structure was covered with elemental calcium and phosphorous on day 30. Color images available online at www.liebertpub.com/scd

analysis did not show peaks for elemental phosphorous and calcium on the cells (Supplementary Fig. S1F).

Ultrastructure of osteogenic MSCs and iPSCs

We further evaluated by electron diffraction analysis whether the osteogenically induced MSCs and iPSCs differentiated sufficiently to show hydroxyapatite formation. TEM images of osteogenically induced MSCs on day 10 showed that the cells were surrounded by fibrous ECM containing electron-dense vesicles (Fig. 5A). Needle-like mineral aggregates were evident in the vesicles (Fig. 5B), which showed partial similarity to hydroxyapatite on SAED analysis. On day 30 of osteogenic induction, electron-dense vesicles were evident immediately outside the cell membrane, within membrane invaginations, and within the cell (Fig. 5C), and the vesicles surrounding the cells showed a diffused diffraction pattern identical to that of typical hydroxyapatite [28] (Fig. 5D).

TEM images of osteogenic iPSCs revealed that a relatively faint electron-dense structure surrounded the cells on day 10 (Fig. 5E). The structure consisted of scattered needle-like minerals (Fig. 5F), and an SAED analysis of the structure indicated a lack of a textured crystalline diffraction pattern. On day 30 of osteogenic iPSC culture, heavily electron-dense vesicles, some of which showed dispersion of their mineral contents, were visible in the extracellular spaces (Fig. 5G). The electron-dense vesicles showed a clear diffraction ring pattern that represented the reflections of hydroxyapatite crystals (Fig. 5H).

Osteogenic gene expression of MSCs and iPSCs

We next examined the gene expression profile during osteogenesis of MSCs and iPSCs. Real-time RT-PCR analysis showed up-regulation of osteogenic genes (*runx2*, osterix, *dlx5*, BSP, and osteocalcin) in both MSCs and iPSCs that are subjected to osteogenic induction (Fig. 6). Specifically, the gene expression profiles of *runx2*, *osterix*, and BSP were similar for both MSCs and iPSCs. In contrast, the gene expression profiles of *dlx5* and osteocalcin were different between iPSCs and MSCs. The increase in gene expression levels of osteogenic marker genes, especially *runx2*, *dlx5*, and osteocalcin, was significantly higher in iPSCs than in MSCs.

We further compared the expression levels of 84 osteogenesis-related genes in MSCs and iPSCs on days 10 and 30 using an osteogenic PCR array analysis. Osteogenic MSCs expressed 85.7% and 89.3% of the 84 osteogenesis-related genes on days 10 and 30, respectively. Osteogenic iPSCs expressed 97.6% and 98.8% of the 84 osteogenesis-related genes on days 10 and 30, respectively. The correlation (Pearson correlation coefficient; r) for osteogenesis-related gene expression between MSCs and iPSCs was 0.81 and 0.78 on days 10 and 30, respectively. On day 10, 14 osteogenesis-related genes were differentially expressed in iPSCs by more

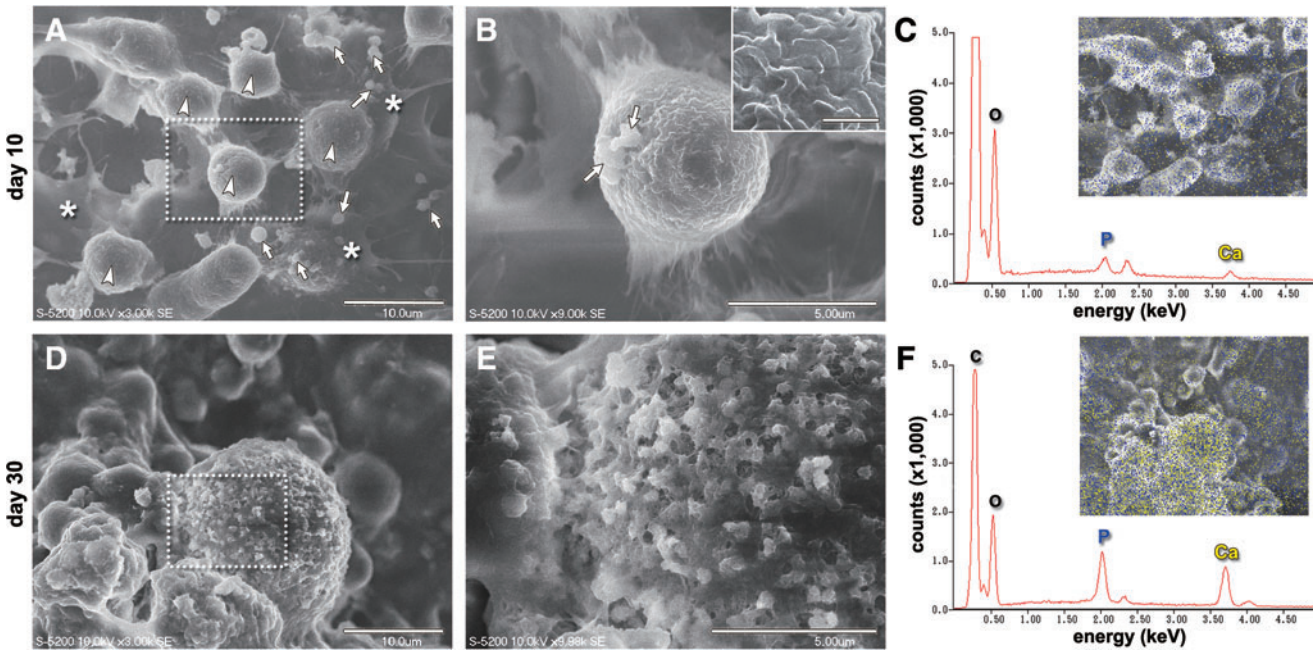

FIG. 4. SEM observation of iPSCs during osteogenic differentiation. **(A–C)** Day 10. **(A)** Rounded cells (*arrowheads*) were growing on the multilayered fibroblastic cells (*asterisks*). Many small globular vesicle structures (*arrows*) were observed on the multilayered fibroblastic cells. Scale bar: 10 μm. **(B)** Magnification of the *dotted square* in **(A)**. Vesicle-like amorphous structures (*arrows*) were budding from the rounded cells. Scale bar: 5 μm. *Inset*: The surface of the rounded cells was covered with many tiny microvillus-like projections (scale bar: 0.5 μm). **(D–F)** Day 30. **(D)** The rounded cells exhibited a rough surface covered by small granulated accretions. Scale bar: 10 μm. **(E)** Magnification of the *dotted square* in **(D)**. The surface of the rounded cells was gritty with ruptured vesicle accretions. Fibrous structures were rarely observed with the accretions. Scale bar: 5 μm. **(C, F)** EDX analyses of the areas shown in SEM images **(A)** and **(D)**, respectively. Energy peaks in the EDX graph correspond to elemental phosphorous (P), calcium (Ca), carbon (C), and oxygen (O). *Insets*: **(C)** Elemental calcium (*yellow dots*) and phosphorous (*blue dots*) were sparsely present on the layered cells on day 10. Accumulation of these elements on the vesicle structures was barely observed. **(F)** Elemental calcium (*yellow dots*) and phosphorous (*blue dots*) intensely accumulated on the surface of the rounded cells by day 30. Color images available online at www.liebertpub.com/scd

than 10-fold compared with MSCs [up-regulated: collagen (*col*) *14a1*, intercellular adhesion molecule 1 (*icam1*), integrin alpha m (*itgam*), alpha-2-HS-glycoprotein (*ahsg*), bone morphogenetic protein (*bmp*) *2*, matrix metallopeptidase (*mmp*) *10*, fibroblast growth factor (*fgf*) *1*, *bmp 6*, tuftelin 1 (*tuft1*), *col 4a1*, and *col 4a2*; down-regulated: *col 12a1*, *mmp 2*, and transforming growth factor beta (*tgfb*) *2*] (Fig. 7A). Only iPSCs and not MSCs expressed cd36 antigen (*cd36*), growth differentiation factor (*gdf*) *10*, *bmp 3*, *fgf 3, bmp 5*, *mmp 9*, sclerostin (*sost*), ameloblastin (*ambn*), tumor necrosis factor (*tnf*), and colony stimulating factor (*csf*) *2*. On day 30, the number of differentially expressed genes in iPSCs compared with MSCs increased to 20 (up-regulated: *icam1*, *col 4a1*, *mmp 10*, *fgf 3*, *ahsg*, *itgam*, *fgf 1*, cathepsin k, *tuft1*, *bmp 6*, *col 14a1*, *tnf*, and *col 4a2*; down-regulated: *col 11a1*, *col 12a1*, *col 1a2*, *col 6a2*, *mmp 2*, *col 1a1*, and *runx2*) (Fig. 7B). iPSCs, but not MSCs, expressed *cd36*, *gdf 10*, *bmp 3*, *bmp 5*, *mmp 9*, and *sost* on day 30.

Discussion

The differences between iPSC-derived osteoblasts and MSC-derived osteoblasts provide a compelling argument for the use of iPSCs in bone tissue engineering. Here, we have assessed the ability of mouse iPSCs to be directionally differentiated to mature osteoblasts in vitro and compared their osteogenic characteristics with those of MSCs. The guided differentiation strategy that we chose to commit the iPSCs to the osteoblast lineage was based on a previous method employing EB formation and subsequent RA treatment [10–13,15]. RA is known to produce immature mesenchymal cells from mouse ESCs via expression of neural crest markers (foxd3 and sox10) and a pre-somatic mesoderm marker (mox1), which provides an origin for mesenchymal elements [23,34]. In this study, soluble factors, including dexamethasone, ascorbic acid, and β-glycerophosphate, were used to induce iPSC osteogenesis after RA treatment. These factors are commonly used for MSC osteogenic induction [9] and have also been shown to be critical for mouse ESCs to acquire the mature osteogenic phenotype [23]. Bilousova et al. [15] demonstrated that RA-treated mouse iPSCs cultured with these osteogenic factors formed calcified structures both in vitro and in vivo.

In preliminary experiments, we assessed two starting culture conditions to optimize the osteogenic induction of iPSCs: (1) direct plating of aggregated EBs on the culture substrate, and (2) plating of individual cells obtained after dissociation of EBs. After 21 days of induction, aggregated iPSCs exhibited robust nodule mineralization as indicated

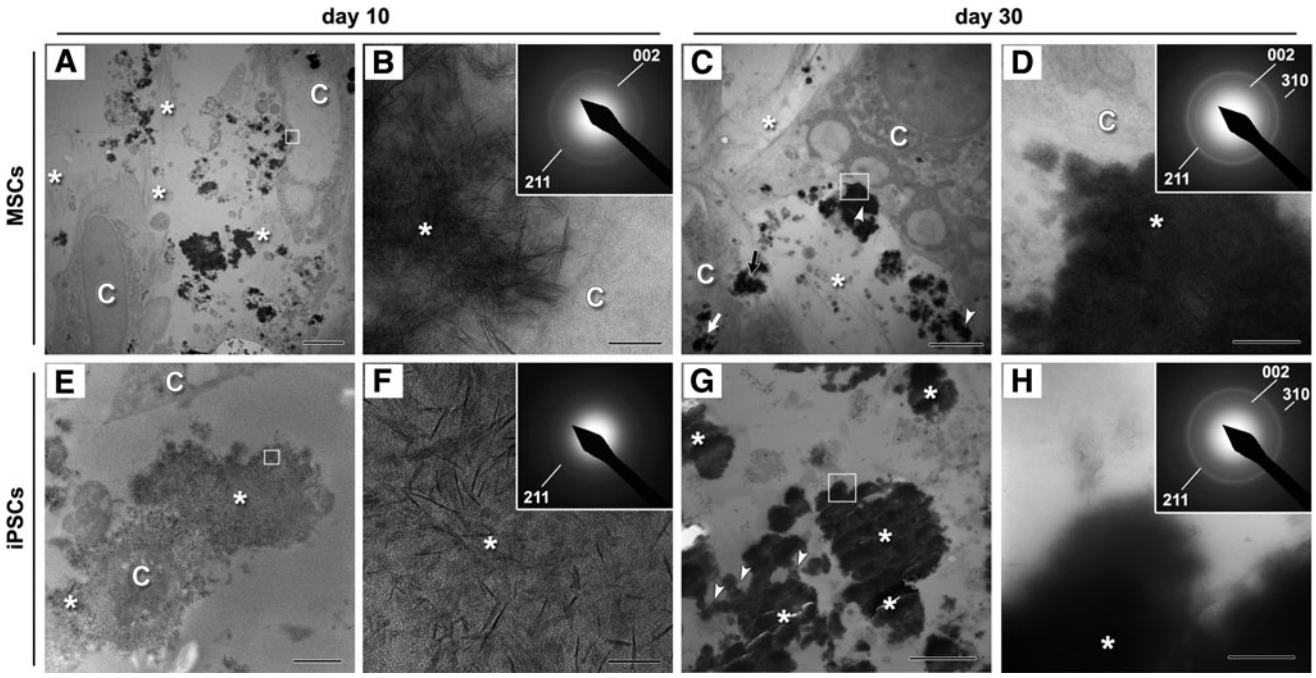

FIG. 5. Transmission electron microscopy images of bone nodules formed in osteogenically induced MSCs **(A–D)** and iPSCs **(E–H)** cultures. Cells are indicated as ''C'' in the panels. **(A)** Cross-section through the MSCs on day 10. Calcium phosphate-containing vesicles (*black spot areas*) were visible around the cells and in the extracellular spaces, which contained fibrous ECM (*asterisks*). Scale bar: 5 μm. **(B)** Magnified image of the *square* in **(A)**. Micrograph showing mineral aggregates (*asterisk*) immediately outside the cell. Scale bar: 100 nm. *Inset*: the selected area electron diffraction (SAED) pattern of the mineral aggregate was similar to that of hydroxyapatite. **(C)** Micrograph of a cross-section through the MSCs on day 30. Electron-dense vesicles (*dense black spots*) were evident immediately outside cells (*arrowheads*), within membrane invaginations (*black arrow*), and within cells (*white arrow*). Fibrous ECM was visible (*asterisks*). Scale bar: 5 μm. **(D)** Magnified image of the *dotted square* in **(C)**. Micrograph showing dense mineral (*asterisk*) immediately outside the cell membrane. Scale bar: 500 nm. *Inset*: SAED analysis of the dense areas was indicative of hydroxyapatite. **(E)** Cross-section through the iPSCs on day 10. An electron-sparse structure (*asterisks*) surrounded the cells. Scale bar: 2 μm. **(F)** Magnified image of the *square* in **(E)**. Electron-dense needle-like minerals are scattered (*asterisk*). Scale bar: 50 nm. *Inset*: SAED analysis of the scattered mineral structure indicated a lack of a textured crystalline diffraction pattern, which suggests that the structure is relatively amorphous and that mineralization has been initiated. **(G)** Cross-section through the bone nodule portion of iPSCs on day 30. Heavily electron-dense vesicles (*asterisks*) were evident in the ECM spaces. A vesicle, which appeared to be dispersing its mineral contents (*arrowheads*), was also visible. Fibrous structures were not evident in the extracellular spaces. Scale bar: 5 μm. **(H)** Magnification of the *dotted square* in **(G)**. The SAED pattern of an electron-dense vesicle (*asterisk*) was identical to that of typical hydroxyapatite (*inset*). Scale bar: 500 nm.

by black von Kossa staining; whereas dissociated iPSCs exhibited brownish staining (data not shown). RT-PCR analysis showed that the expression of osteogenic marker genes, such as *runx2*, osterix, *col 1a2*, and BSP, was significantly higher in aggregated iPSC cultures than in dissociated iPSC cultures (data not shown), suggesting that aggregated EB culture markedly enhances iPSC osteogenic differentiation. Therefore, we chose to directly apply osteogenic induction to attached EBs in all subsequent experiments, because the use of suspended dissociated iPSCs rather than EBs would not represent the full potential of iPSC osteogenesis and, furthermore, would not reflect the protocol likely to be used when iPSCs are actually applied to bone tissue engineering. However, it should be simultaneously noted that the study design did not permit a perfectly direct comparison because of the use of aggregated iPSCs and dispersed MSCs. Therefore, our focus on using the most therapeutically relevant iPSC differentiation conditions prevented us from addressing distinct mechanisms underlying the observed osteogenesis. Another limitation of this study is that the cell seeding density was relatively higher than that in typical osteogenic differentiation studies [35–38]; thus, the optimal seeding density for a direct comparison of MSCs and iPSCs should be explored.

An alternative strategy would be to isolate putative MSCs from pluripotent stem cells, which provides the advantage of producing a large source of osteoblasts [39,40] and would, thus, be particularly useful for restoring tissue function with implantable, laboratory-grown constructs that contain tissue-specific cells [41]. However, in the present study, we reasoned that if iPSCs could be directly guided into mature osteoblasts which produce bone matrices with the mineral composition of native bone (without requiring an interim MSC differentiation/isolation step), the resulting artificially produced osteoblasts could more easily be used to prepare tissue-engineered constructs, as there would be no need for time-consuming and costly isolation and expansion of putative MSCs from the original iPSC population. This approach would also harness the innate benefit of iPSCs, that is, the provision of an unlimited cell source, because iPSCs

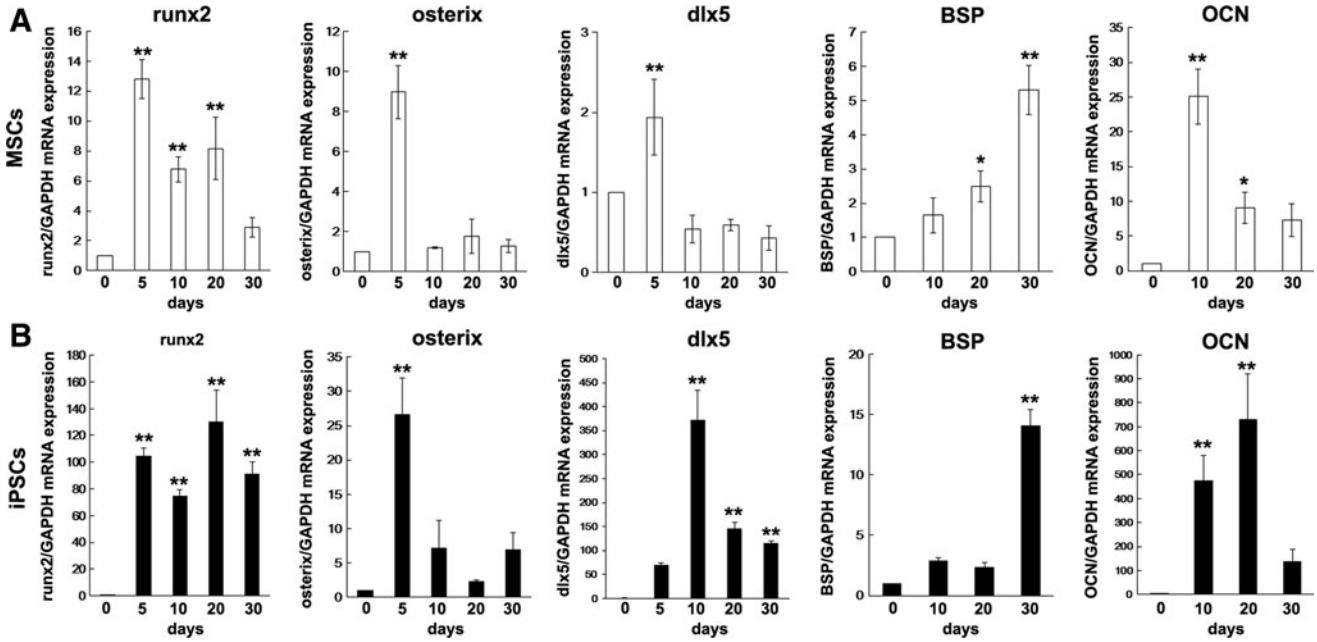

FIG. 6. Expression of osteogenic marker genes in MSCs **(A)** and iPSCs **(B)**. Expression of osteogenic marker genes *runx2*, osterix, *dlx5*, bone sialoprotein (BSP), and osteocalcin (OCN) during osteogenic induction for 30 days was assessed by real-time reverse transcription–polymerase chain reaction (RT-PCR) analysis. Gene expression of glyceraldehyde-3-phosphate dehydrogenase (*GAPDH*) was used as an internal control. The data represent the mean values ± SD ($n = 3$). Significant differences (**$P < 0.01$, *$P < 0.05$: ANOVA with Dunnett's correction for multiple comparisons) were evaluated with regard to the day 0 (before osteogenic induction) values.

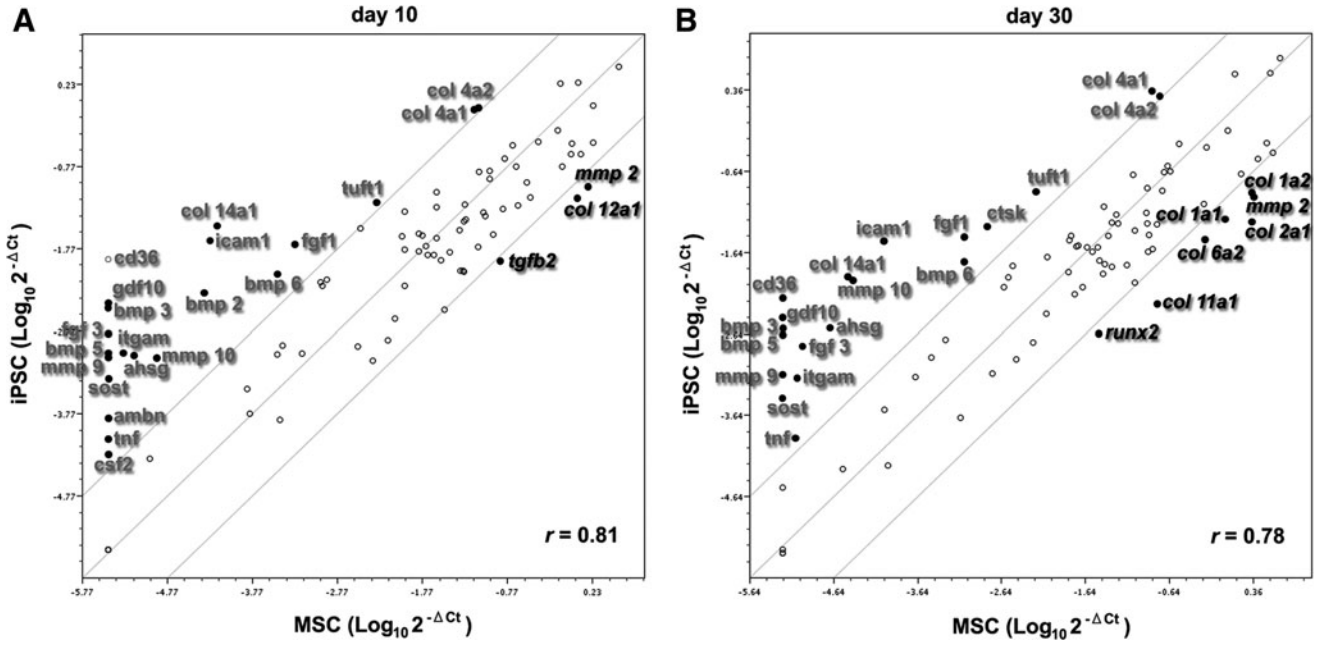

FIG. 7. Comparative expression analysis of osteogenesis-related genes between iPSCs and MSCs. Expression of 84 osteogenesis-related genes (listed in the Supplementary Table S1) on days 10 **(A)** and 30 **(B)** of osteogenic induction was evaluated using real-time RT-PCR array analysis (Mouse Osteogenesis RT^2 Profiler PCR Array: Qiagen). Expression levels ($2^{-\Delta CT}$) of these genes are plotted on a logarithmic scale. The two boundary lines above and below the center partition line indicate the threshold of 10-fold up-regulation and down-regulation in iPSCs relative to MSCs. Genes with at least 10-fold higher (*in gray*) or lower (*in italics*) expression in iPSCs compared with MSCs are shown as *black dots* (the gene names for the abbreviations are given in Supplementary Table S1). The Pearson correlation coefficients (r) of the spotted genes are indicated.

are self-renewing pluripotent stem cells, and the resulting three-dimensional calcified cell construct may facilitate cell transplantation without the need for artificially synthesized scaffolds.

Indeed, our results show that this simple induction method guides the differentiation of iPSCs to produce robust ECM mineralization. Furthermore, the osteoblast lineage in the present study was defined by increased expression of essential osteogenic marker genes. *Runx2* encodes one of the earliest master transcription factors that directs the differentiation of stem cells into osteoblasts and triggers the expression of major bone matrix genes [42]. In addition to *runx2*, osterix and *dlx5* encode transcription factors that are indispensable coordinators of osteoblast differentiation [43,44] and are expressed in the early stages of osteogenic differentiation of MSCs [45]. BSP and osteocalcin are bone matrix genes that are expressed in the later stages of osteogenic differentiation [44]. We consistently observed increased expression of osteogenic transcription factors within 10 days and of bone matrix genes after 10 days during osteogenic differentiation of MSCs and iPSCs. The delayed expression of *dlx5*, BSP, and osteocalcin in iPSCs compared with MSCs may be related to differences in the cell seeding protocol and/or the different nature of these stem cells (ie, pluripotent stem cells *vs*. multipotent stem cells). Nonetheless, these results suggest that similar to MSCs, iPSCs require expression of these indispensable osteogenic marker genes when undergoing osteogenesis.

The PCR array analysis for osteogenesis confirmed robust expression of $\sim$86% and 99% of osteogenesis-related genes in the array in late-osteogenic MSCs and iPSCs, respectively. Guided differentiation of MSCs and iPSCs into mature osteoblasts was further supported by the observation of increased calcium deposition. In addition, the FTIR spectral pattern of the mineralized iPSCs was identical to that of the mineralized MSCs, showing clear absorption peaks for bone-related phosphate, carbon, and amino acids. In the mineralized MSCs and iPSCs, the EDX spectrum displayed high peaks corresponding to elemental phosphorous and calcium. These results suggest that osteogenically induced MSCs and iPSCs produce constituents of bone, especially abundant calcium phosphate, which is a major component of hydroxyapatite. We further confirmed the actual occurrence of hydroxyapatite formation in these cell types by SAED analysis, which detected a clear diffraction ring pattern that represented the reflections of hydroxyapatite crystals. These results suggest that the conventional osteogenic induction method for MSCs facilitates the differentiation of RA-treated mouse iPSCs into mature osteoblasts which are associated with a hydroxyapatite crystal structure. To our knowledge, this is the first report showing a hydroxyapatite crystal structure, which is the in vitro hallmark of mature functional osteoblasts, in osteogenically induced iPSCs. Our results also demonstrate that iPSC EBs can be directly guided into mature osteoblasts which produce bone matrices with the mineral composition of native bone. This finding may lead to a new strategy to apply these directly induced osteogenic iPSCs and produce substrate materials for laboratory-grown constructs for bone regeneration.

Although our data show that iPSCs and MSCs possess a comparable osteogenic differentiation capacity, the proliferation behavior and calcification process during osteogenic differentiation appear to be different between MSCs and iPSCs. MSCs at the early induction stage presented an elongated shape and formed a confluent mono-layer, and the mineralized areas at the late induction stage were evenly distributed over the MSC cultures. The mono-layer structure provided by the homogeneous elongated shape of the MSCs created a uniform extracellular space for matrix vesicle deposition, thus explaining the even distribution of the subsequently formed mineralized zones. When iPSCs at the early induction stage were observed under electron microscopy, abundant proliferating small rounded cells existed on three-dimensional aggregates of cells. High proliferation and self-organization are intrinsic, defining characteristics of pluripotent stem cells [46,47] that may enable iPSC aggregates to proliferate three dimensionally during the initial induction stage and form studded dense multi-layer spots on the culture plate. Microscopic observation of von Kossa staining showed that the iPSC aggregates were well stained on day 20, and mineralization appeared to propagate from the aggregates on day 30. These observations are in accord with the macroscopic visual inspection of von Kossa staining, which showed studded mineralized areas in the iPSC cultures. Aggregation of ESCs increases mesodermal homogeneity, which enhances osteogenic differentiation in vitro [48]. In addition, altered internal mechanisms of iPSC aggregates may accelerate osteogenic differentiation, possibly by affecting compaction, condensation, and mechanical stress. The enhancement of iPSC osteogenesis by three-dimensional aggregation, therefore, likely contributed to the observed increase in calcium deposition relative to monolayer MSCs. These data support previous reports indicating a superior ability of ESCs to produce a mineralized matrix relative to MSCs [49,50].

Osteoblasts create the nano-composite structure of bone by secreting a collagenous ECM on which apatite crystals subsequently form [51]. In the present study, SEM observation suggested that calcified MSCs and iPSCs were different at the late induction stage. Calcified MSCs presented a flat and solid structure with a relatively smooth surface (Fig. 3D), whereas rounded iPSCs on cell aggregates exhibited robust calcification with abundant small granulated accretions, which represents calcification with a gritty surface texture (Fig. 4D). Various mechanisms have been proposed to explain early bone mineral formation, including (i) transport of amorphous calcium phosphate and ionic calcium stored in cells through vesicles to the ECM, followed by deposition on collagen fibrils and conversion to additional crystalline apatite [51], and (ii) a cell-controlled mechanism by which vesicles that bud from the plasma membrane accumulate ions extracellularly, mediate calcium phosphate precipitation, and subsequently rupture, thereby dispersing their contents on the ECM [52].

According to present findings, the bone mineral formation process of MSCs is likely to follow mechanism (i) above. TEM observation of osteogenic MSCs demonstrated that vesicles enclosing electron-dense mineral aggregates were present within cells, within membrane invaginations, and immediately outside plasma membranes (Fig. 5C). SEM observation of MSCs at the early induction stage suggested that the vesicles outside plasma membranes were deposited on abundant collagen fibrils (Fig. 3A, B). These deposits contained mineral aggregates (Fig. 5B) that appeared to be

converted to additional crystalline apatite (Fig. 5D) at the late induction stage to form a solid structure in the extracellular space (Fig. 3D, E).

In contrast, mineral formation of iPSCs at the early induction stage likely follows mechanism (ii) above, as many amorphous vesicles including matrix vesicles budding from the cell membrane were observed on day 10 (Fig. 4A, B). These vesicles appear to mainly accumulate calcium phosphate ions extracellularly, because the EDX analysis showed little specific localization of elemental calcium and phosphorous in the vesicles (Fig. 4C). TEM/SAED also showed a scattered mineral structure surrounding iPSCs that lacked a textured crystalline diffraction pattern, which suggests that the structure was amorphous and that further mineralization was initiated (Fig. 5E, F). Once the iPSCs acquired a mature osteogenic phenotype by day 30, a gritty mineralized structure (Fig. 4E) with crystalline apatite (Fig. 5H) covered them, possibly through rupture of the mineralized vesicles and subsequent dispersal of their mineral contents (Fig. 5G). It should be also noted that a lower amount of fibril structures in extracellular spaces was evident in iPSCs relative to MSCs. The observed mineralization of iPSCs was similar to that in ESCs; that is, limited type I collagen was present in the ECM despite abundant mineral deposition [49]. Our findings suggest that bone nodule formation by mouse iPSCs may occur in large part through a mechanism other than collagen fibril-mediated mineralization, as previously observed for mouse ESCs [41].

The different matrix calcification properties between MSCs and iPSCs were associated with different expression patterns of osteogenesis-related genes during osteogenic differentiation. The PCR array analysis demonstrated significant differences with regard to expression of osteogenesis-related genes between iPSCs and MSCs subjected to osteogenic induction. In particular, osteogenic iPSCs showed significantly higher expression of several mineralization-associated molecules, such as *ahsg* (also known as fetuin-A), *sost*, *tuft1*, and *ambn*, compared with osteogenic MSCs. The plasma protein ahsg is a mineral chaperone [53] mediating the transport of minerals from the extracellular space. Sclerostin, a product of the *sost* gene, is a regulator of late-osteoblast/preosteocyte differentiation and it regulates mineralization [54]. Although ahsg and sost are potent inhibitors of mineralization [54,55], they are highly expressed by mature osteoblasts and osteocytes [56,57], and they may protect mature osteoblasts from lethally excessive calcification [58]. Tuft1 and ambn were originally found in the mature extracellular enamel of teeth [59,60], and they play an important role in enamel mineralization [61,62]. Ambn is also expressed in osteoblasts and promotes osteogenic differentiation [63,64]. High expression of these mineralization-associated molecules in osteogenic iPSCs may partly explain our findings and those of previous reports [49,50], indicating a superior ability of iPSCs or ESCs to produce a mineralized matrix relative to MSCs.

Other skeletal development-associated genes with high expression in osteogenic iPSCs include those encoding BMPs, such as *bmp 2*, *bmp 3*, *bmp 5*, and *bmp 6*. BMP 2, BMP 5, and BMP 6 are among the most potent inducers and stimulators of osteoblast differentiation [65–68]. For normal osteogenesis to proceed, the expression of BMPs needs to be suppressed, as observed in human ESCs during osteogenic differentiation [69]. BMP 3 is produced by osteoblasts and osteocytes in vivo as a means of regulating adult bone mass, in which it suppresses osteoblast differentiation induced by other BMPs [70]. The high expression of a set of BMP-encoding genes including *bmp 3* in osteogenic iPSCs may, in part, support their osteogenesis and maintenance of mature osteoblast phenotypes.

It should be also noted that the gene expression of ECM collagens was different between osteogenic MSCs and iPSCs. Osteogenic iPSCs showed significantly lower gene expression of *col 1a1* and *col 1a2*, which encode the main components of the matrix fibrils produced by bone-forming cells [71], than MSCs. Mature osteogenic mouse ESCs express col 1a1 at a significantly lower level than calvarial osteoblasts and MSCs [41,49]. The low expression of these fibril-forming type 1 collagens by osteogenic iPSCs explains the lower amount of fibril structures in their extracellular spaces relative to osteogenic MSCs as observed in our SEM/TEM studies. In the present study, osteogenic MSCs highly expressed cartilage-associated collagens [72], such as *col 2a1*, *col 6a2*, *col 11a1*, and *col 12a1*, which is in accord with previous reports, suggesting intrinsic expression of chondrogenic genes during osteogenesis of bone marrow-derived MSCs [41,73,74]. In contrast, osteogenic iPSCs highly expressed *col 4a1* and *col 4a2*, which encode major constituents of the basement membrane, and *col 14a1*, which encodes an FACIT (fibrillar-associated collagen with interrupted triple-helix) that is widely expressed in several tissues, including bone [72]. Although these osteogenesis-related collagens were expressed in both osteogenic MSCs and iPSCs, the differences in expression level for each collagen between cell types may have resulted in constitutional differences in the respective ECMs, thus leading to cell-specific differences in nanolevel architecture and complex biomolecular and mineral composition. Based on an FTIR spectral analysis, Shimko et al. [49] reported that the minerals deposited in vitro by osteogenic mouse ESCs more closely approximated normal bone tissue than minerals deposited by MSCs. With regard to the architecture of the bone nodules, Gentleman et al. [41] reported that mineral crystallites in the bone nodules of calvarial osteoblasts are associated with collagen fibrils, whereas bone nodules of ESCs lack connectivity between the mineral and fibrous proteins, thereby significantly affecting their mechanical properties.

It should be noted that the expression of *runx2*, which encodes a key osteogenic transcription factor controlling the expression of *col 1a1* and BSPs, was significantly lower in osteogenic iPSCs than in osteogenic MSCs. Osteogenic ESCs express significantly lower levels of the *runx2* gene than calvarial osteoblasts and MSCs [41,50]. Although *runx2* expression was significantly lower in osteogenic iPSCs than in MSCs, real-time RT-PCR showed that *runx2* expression in undifferentiated iPSCs (''day 0'' of induction) increased by more than 60-fold during differentiation to the mature osteogenic phenotype; whereas *runx2* expression in MSCs increased by 13-fold. This 60-fold increase in transcriptional factor expression may be sufficient to guide undifferentiated iPSCs to an osteogenic lineage and mature osteoblast phenotypes.

Our results imply that some of the underlying osteogenic differentiation mechanisms are different between iPSCs and MSCs, possibly because the osteogenesis process of iPSCs

includes a pluripotent stem cell-specific osteogenic step in which iPSCs are committed to become mesenchymal cells. The heterogeneous nature of the iPSCs may, in part, have influenced the observed expression differences between iPSCs and MSCs. However, the ultrastructural analysis also clearly demonstrated different matrix calcification properties between iPSCs and MSCs; therefore, the observed difference in gene expression patterns more likely represents a difference in the intrinsic properties of both stem cell types.

It is uncertain at this point whether iPSCs from female mice show the same osteogenic differentiation behavior as iPSCs from male mice. In the mouse system, female iPSCs show reactivation of a somatically silenced X chromosome [75], implying that both male and female iPSCs would be similar to ES cells not only at the transcriptome level but also in their epigenetic signature. However, Anguera et al. [76] recently demonstrated sex-specific differences in human iPSCs, where female iPSCs were found to be epigenetically less stable. Osteoporosis is a critical bone health problem in menopausal women; therefore, it will be important to recapitulate the osteogenic differentiation ability in iPSCs from female cells to study this disease.

Taken together, these results suggest that iPSCs are capable of differentiation into mature osteoblasts whose associated hydroxyapatite has a crystal structure similar to that of MSC-associated hydroxyapatite; however, the transcriptional differences between the cell types imply differences in the mineral and matrix environments of the bone nodules. Direct comparison studies are indispensable for future implementation of iPSCs in regenerative medicine. To our knowledge, our study is the first that compares the osteogenic differentiation and mineralization of MSCs and iPSCs by culturing the cells under identical conditions; clear differences were observed in mineralization properties along with differences in osteogenic-related gene expression. A better understanding of these osteogenic processes will contribute to clinical success in the long term.

Acknowledgments

The authors thank Takao Sakata and Tomoki Nishida (Osaka University Research Center for ultra-high-voltage electron microscopy) for technical assistance in electron microscope observations. This investigation was supported by Grants-in-Aid for Exploratory Research (24659858, H.E.) and for Scientific Research (A: 25253102, H.Y. and H.E.; and B: 25293395, H.E.) from the Japan Society for the Promotion of Science.

Author Disclosure Statement

No competing financial interests exist.

References

1. Greenwald AS, SD Boden, VM Goldberg, Y Khan, CT Laurencin and RN Rosier. (2001). Bone-graft substitutes: facts, fictions, and applications. J Bone Joint Surg Am 83-A Suppl 2 Pt 2:98–103.
2. De Long WG, Jr., TA Einhorn, K Koval, M McKee, W Smith, R Sanders and T Watson. (2007). Bone grafts and bone graft substitutes in orthopaedic trauma surgery. A critical analysis. J Bone Joint Surg Am 89:649–658.
3. Egusa H. (2012). iPS cells in dentistry. Clin Calcium 22:67–73.
4. Egusa H, W Sonoyama, M Nishimura, I Atsuta and K Akiyama. (2012). Stem cells in dentistry—Part II: clinical applications. J Prosthodont Res 56:229–248.
5. Meijer GJ, JD de Bruijn, R Koole and CA van Blitterswijk. (2007). Cell-based bone tissue engineering. PLoS Med 4:e9.
6. Takahashi K and S Yamanaka. (2006). Induction of pluripotent stem cells from mouse embryonic and adult fibroblast cultures by defined factors. Cell 126:663–676.
7. Takahashi K, K Tanabe, M Ohnuki, M Narita, T Ichisaka, K Tomoda and S Yamanaka. (2007). Induction of pluripotent stem cells from adult human fibroblasts by defined factors. Cell 131:861–872.
8. Egusa H, W Sonoyama, M Nishimura, I Atsuta and K Akiyama. (2012). Stem cells in dentistry—part I: stem cell sources. J Prosthodont Res 56:151–165.
9. Vater C, P Kasten and M Stiehler. (2011). Culture media for the differentiation of mesenchymal stromal cells. Acta Biomater 7:463–477.
10. Tashiro K, M Inamura, K Kawabata, F Sakurai, K Yamanishi, T Hayakawa and H Mizuguchi. (2009). Efficient adipocyte and osteoblast differentiation from mouse induced pluripotent stem cells by adenoviral transduction. Stem Cells 27:1802–1811.
11. Li F, S Bronson and C Niyibizi. (2010). Derivation of murine induced pluripotent stem cells (iPS) and assessment of their differentiation toward osteogenic lineage. J Cell Biochem 109:643–652.
12. Li F and C Niyibizi. (2012). Cells derived from murine induced pluripotent stem cells (iPSC) by treatment with members of TGF-beta family give rise to osteoblasts differentiation and form bone *in vivo*. BMC Cell Biol 13:35.
13. Okamoto H, Y Matsumi, Y Hoshikawa, K Takubo, K Ryoke and G Shiota. (2012). Involvement of microRNAs in regulation of osteoblastic differentiation in mouse induced pluripotent stem cells. PLoS One 7:e43800.
14. Kao CL, LK Tai, SH Chiou, YJ Chen, KH Lee, SJ Chou, YL Chang, CM Chang, SJ Chen, HH Ku and HY Li. (2010). Resveratrol promotes osteogenic differentiation and protects against dexamethasone damage in murine induced pluripotent stem cells. Stem Cells Dev 19:247–258.
15. Bilousova G, H Jun du, KB King, S De Langhe, WS Chick, EC Torchia, KS Chow, DJ Klemm, DR Roop and SM Majka. (2011). Osteoblasts derived from induced pluripotent stem cells form calcified structures in scaffolds both *in vitro* and *in vivo*. Stem Cells 29:206–216.
16. Hayashi T, H Misawa, H Nakahara, H Noguchi, A Yoshida, N Kobayashi, M Tanaka and T Ozaki. (2012). Transplantation of osteogenically differentiated mouse iPS cells for bone repair. Cell Transplant 21:591–600.
17. Bonewald LF, SE Harris, J Rosser, MR Dallas, SL Dallas, NP Camacho, B Boyan and A Boskey. (2003). von Kossa staining alone is not sufficient to confirm that mineralization *in vitro* represents bone formation. Calcif Tissue Int 72:537–547.
18. Egusa H, K Okita, H Kayashima, G Yu, S Fukuyasu, M Saeki, T Matsumoto, S Yamanaka and H Yatani. (2010). Gingival fibroblasts as a promising source of induced pluripotent stem cells. PLoS One 5:e12743.
19. Egusa H, M Kobayashi, T Matsumoto, J Sasaki, S Uraguchi and H Yatani. (2013). Application of cyclic strain for accelerated skeletal myogenic differentiation of mouse bone

marrow-derived mesenchymal stromal cells with cell alignment. Tissue Eng Part A 19:770–782.
20. Sasaki J, T Matsumoto, H Egusa, M Matsusaki, A Nishiguchi, T Nakano, M Akashi, S Imazato and H Yatani. (2012). *In vitro* reproduction of endochondral ossification using a 3D mesenchymal stem cell construct. Integr Biol 4:1207–1214.
21. Egusa H, FE Schweizer, CC Wang, Y Matsuka and I Nishimura. (2005). Neuronal differentiation of bone marrow-derived stromal stem cells involves suppression of discordant phenotypes through gene silencing. J Biol Chem 280: 23691–23697.
22. Itskovitz-Eldor J, M Schuldiner, D Karsenti, A Eden, O Yanuka, M Amit, H Soreq and N Benvenisty. (2000). Differentiation of human embryonic stem cells into embryoid bodies compromising the three embryonic germ layers. Mol Med 6:88–95.
23. Kawaguchi J, PJ Mee and AG Smith. (2005). Osteogenic and chondrogenic differentiation of embryonic stem cells in response to specific growth factors. Bone 36:758–769.
24. Egusa H, Y Kaneda, Y Akashi, Y Hamada, T Matsumoto, M Saeki, DK Thakor, Y Tabata, N Matsuura and H Yatani. (2009). Enhanced bone regeneration via multimodal actions of synthetic peptide SVVYGLR on osteoprogenitors and osteoclasts. Biomaterials 30:4676–4686.
25. Matsumoto M, J Miura, F Takeshige and H Yatani. (2013). Mechanical and morphological evaluation of the bond-dentin interface in direct resin core build-up method. Dental Mater 29:287–293.
26. Shivali G, L Praful and G Vijay. (2012). A validated Fourier transform infrared spectroscopy method for quantification of total lactones in *Inula racemosa* and *Andrographis paniculata*. Phytochem Anal 23:171–176.
27. Sato T. (1968). A modified method for lead staining of thin sections. J Eelectron Microsc 17:158–159.
28. Kim YK, LS Gu, TE Bryan, JR Kim, L Chen, Y Liu, JC Yoon, L Breschi, DH Pashley and FR Tay. (2010). Mineralisation of reconstituted collagen using polyvinylphosphonic acid/polyacrylic acid templating matrix protein analogues in the presence of calcium, phosphate and hydroxyl ions. Biomaterials 31:6618–6627.
29. Liu Y, YK Kim, L Dai, N Li, SO Khan, DH Pashley and FR Tay. (2011). Hierarchical and non-hierarchical mineralisation of collagen. Biomaterials 32:1291–1300.
30. Schmittgen TD and KJ Livak. (2008). Analyzing real-time PCR data by the comparative C(T) method. Nat Protoc 3: 1101–1108.
31. Buttery LD, S Bourne, JD Xynos, H Wood, FJ Hughes, SP Hughes, V Episkopou and JM Polak. (2001). Differentiation of osteoblasts and *in vitro* bone formation from murine embryonic stem cells. Tissue Eng 7:89–99.
32. Schoeters GE, L de Saint-Georges, R Van den Heuvel and O Vanderborght. (1988). Mineralization of adult mouse bone marrow *in vitro*. Cell Tissue Kinet 21:363–374.
33. Boskey A and N Pleshko Camacho. (2007). FT-IR imaging of native and tissue-engineered bone and cartilage. Biomaterials 28:2465–2478.
34. Kawaguchi J. (2006). Generation of osteoblasts and chondrocytes from embryonic stem cells. Methods Mol Biol 330:135–148.
35. McCulloch CA, M Strugurescu, F Hughes, AH Melcher and JE Aubin. (1991). Osteogenic progenitor cells in rat bone marrow stromal populations exhibit self-renewal in culture. Blood 77:1906–1911.
36. Jaiswal N, SE Haynesworth, AI Caplan and SP Bruder. (1997). Osteogenic differentiation of purified, culture-expanded human mesenchymal stem cells *in vitro*. J Cell Biochem 64:295–312.
37. Purpura KA, JE Aubin and PW Zandstra. (2004). Sustained *in vitro* expansion of bone progenitors is cell density dependent. Stem Cells 22:39–50.
38. Aubin JE. (1999). Osteoprogenitor cell frequency in rat bone marrow stromal populations: role for heterotypic cell-cell interactions in osteoblast differentiation. J Cell Biochem 72:396–410.
39. Brown SE, W Tong and PH Krebsbach. (2009). The derivation of mesenchymal stem cells from human embryonic stem cells. Cells Tissues Organs 189:256–260.
40. Arpornmaeklong P, SE Brown, Z Wang and PH Krebsbach. (2009). Phenotypic characterization, osteoblastic differentiation, and bone regeneration capacity of human embryonic stem cell-derived mesenchymal stem cells. Stem Cells Dev 18:955–968.
41. Gentleman E, RJ Swain, ND Evans, S Boonrungsiman, G Jell, MD Ball, TA Shean, ML Oyen, A Porter and MM Stevens. (2009). Comparative materials differences revealed in engineered bone as a function of cell-specific differentiation. Nat Mater 8:763–770.
42. Komori T. (2010). Regulation of osteoblast differentiation by Runx2. Adv Exp Med Biol 658:43–49.
43. Matsubara T, K Kida, A Yamaguchi, K Hata, F Ichida, H Meguro, H Aburatani, R Nishimura and T Yoneda. (2008). BMP2 regulates Osterix through Msx2 and Runx2 during osteoblast differentiation. J Biol Chem 283:29119–29125.
44. Ryoo HM, MH Lee and YJ Kim. (2006). Critical molecular switches involved in BMP-2-induced osteogenic differentiation of mesenchymal cells. Gene 366:51–57.
45. Liu G, S Vijayakumar, L Grumolato, R Arroyave, H Qiao, G Akiri and SA Aaronson. (2009). Canonical Wnts function as potent regulators of osteogenesis by human mesenchymal stem cells. J Cell Biol 185:67–75.
46. Eiraku M, N Takata, H Ishibashi, M Kawada, E Sakakura, S Okuda, K Sekiguchi, T Adachi and Y Sasai. (2011). Self-organizing optic-cup morphogenesis in three-dimensional culture. Nature 472:51–56.
47. Suga H, T Kadoshima, M Minaguchi, M Ohgushi, M Soen, T Nakano, N Takata, T Wataya, K Muguruma, et al. (2011). Self-formation of functional adenohypophysis in three-dimensional culture. Nature 480:57–62.
48. Gothard D, SJ Roberts, KM Shakesheff and LD Buttery. (2010). Engineering embryonic stem-cell aggregation allows an enhanced osteogenic differentiation *in vitro*. Tissue Eng Part C Methods 16:583–595.
49. Shimko DA, CA Burks, KC Dee and EA Nauman. (2004). Comparison of *in vitro* mineralization by murine embryonic and adult stem cells cultured in an osteogenic medium. Tissue Eng 10:1386–1398.
50. Bigdeli N, GM de Peppo, M Lenneras, P Sjovall, A Lindahl, J Hyllner and C Karlsson. (2010). Superior osteogenic capacity of human embryonic stem cells adapted to matrix-free growth compared to human mesenchymal stem cells. Tissue Eng Part A 16:3427–3440.
51. Boonrungsiman S, E Gentleman, R Carzaniga, ND Evans, DW McComb, AE Porter and MM Stevens. (2012). The role of intracellular calcium phosphate in osteoblast-mediated bone apatite formation. Proc Natl Acad Sci U S A 109:14170–14175.
52. Anderson HC. (1995). Molecular biology of matrix vesicles. Clin Orthop Relat Res 314: 266–280.

53. Jahnen-Dechent W, C Schafer, M Ketteler and MD McKee. (2008). Mineral chaperones: a role for fetuin-A and osteopontin in the inhibition and regression of pathologic calcification. J Mol Med 86:379–389.
54. Atkins GJ, PS Rowe, HP Lim, KJ Welldon, R Ormsby, AR Wijenayaka, L Zelenchuk, A Evdokiou and DM Findlay. (2011). Sclerostin is a locally acting regulator of late-osteoblast/preosteocyte differentiation and regulates mineralization through a MEPE-ASARM-dependent mechanism. J Bone Miner Res 26:1425–1436.
55. Schafer C, A Heiss, A Schwarz, R Westenfeld, M Ketteler, J Floege, W Muller-Esterl, T Schinke and W Jahnen-Dechent. (2003). The serum protein alpha 2-Heremans-Schmid glycoprotein/fetuin-A is a systemically acting inhibitor of ectopic calcification. J Clin Invest 112:357–366.
56. Coen G, P Ballanti, G Silvestrini, D Mantella, M Manni, S Di Giulio, S Pisano, M Leopizzi, G Di Lullo and E Bonucci. (2009). Immunohistochemical localization and mRNA expression of matrix Gla protein and fetuin-A in bone biopsies of hemodialysis patients. Virchows Arch 454:263–271.
57. van Bezooijen RL, BA Roelen, A Visser, L van der Wee-Pals, E de Wilt, M Karperien, H Hamersma, SE Papapoulos, P ten Dijke and CW Lowik. (2004). Sclerostin is an osteocyte-expressed negative regulator of bone formation, but not a classical BMP antagonist. J Exp Med 199:805–814.
58. Schinke T, C Amendt, A Trindl, O Poschke, W Muller-Esterl and W Jahnen-Dechent. (1996). The serum protein alpha2-HS glycoprotein/fetuin inhibits apatite formation *in vitro* and in mineralizing calvaria cells. A possible role in mineralization and calcium homeostasis. J Biol Chem 271:20789–20796.
59. Krebsbach PH, SK Lee, Y Matsuki, CA Kozak, KM Yamada and Y Yamada. (1996). Full-length sequence, localization, and chromosomal mapping of ameloblastin. A novel tooth-specific gene. J Biol Chem 271:4431–4435.
60. Deutsch D, A Palmon, LW Fisher, N Kolodny, JD Termine and MF Young. (1991). Sequencing of bovine enamelin (''tuftelin'') a novel acidic enamel protein. J Biol Chem 266:16021–16028.
61. Mao Z, B Shay, M Hekmati, E Fermon, A Taylor, L Dafni, K Heikinheimo, J Lustmann, LW Fisher, MF Young and D Deutsch. (2001). The human tuftelin gene: cloning and characterization. Gene 279:181–196.
62. Hatakeyama J, S Fukumoto, T Nakamura, N Haruyama, S Suzuki, Y Hatakeyama, L Shum, CW Gibson, Y Yamada and AB Kulkarni. (2009). Synergistic roles of amelogenin and ameloblastin. J Dent Res 88:318–322.
63. Iizuka S, Y Kudo, M Yoshida, T Tsunematsu, Y Yoshiko, T Uchida, I Ogawa, M Miyauchi and T Takata. (2011). Ameloblastin regulates osteogenic differentiation by inhibiting Src kinase via cross talk between integrin beta1 and CD63. Mol Cell Biol 31:783–792.
64. Spahr A, SP Lyngstadaas, I Slaby and G Pezeshki. (2006). Ameloblastin expression during craniofacial bone formation in rats. Eur J Oral Sci 114:504–511.
65. Yamaguchi A, T Komori and T Suda. (2000). Regulation of osteoblast differentiation mediated by bone morphogenetic proteins, hedgehogs, and Cbfa1. Endocr Rev 21:393–411.
66. Cheng H, W Jiang, FM Phillips, RC Haydon, Y Peng, L Zhou, HH Luu, N An, B Breyer, et al. (2003). Osteogenic activity of the fourteen types of human bone morphogenetic proteins (BMPs). J Bone Joint Surg Am 85-A:1544–1552.
67. Ayala-Pena VB, LA Scolaro and GE Santillan. (2013). ATP and UTP stimulate bone morphogenetic protein-2,-4 and -5 gene expression and mineralization by rat primary osteoblasts involving PI3K/AKT pathway. Exp Cell Res 319:2028–2036.
68. Wutzl A, W Brozek, I Lernbass, M Rauner, G Hofbauer, C Schopper, F Watzinger, M Peterlik and P Pietschmann. (2006). Bone morphogenetic proteins 5 and 6 stimulate osteoclast generation. J Biomed Mater Res A 77:75–83.
69. Karner E, C Unger, AJ Sloan, L Ahrlund-Richter, RV Sugars and M Wendel. (2007). Bone matrix formation in osteogenic cultures derived from human embryonic stem cells *in vitro*. Stem Cells Dev 16:39–52.
70. Kokabu S, L Gamer, K Cox, J Lowery, K Tsuji, R Raz, A Economides, T Katagiri and V Rosen. (2012). BMP3 suppresses osteoblast differentiation of bone marrow stromal cells via interaction with Acvr2b. Mol Endocrinol 26:87–94.
71. Eyre DR and JJ Wu. (2005). Collagen cross-links. In: *Collagen*. Brinckmann J, Notbohm H, Müller PK, eds. Springer, Berlin, pp 207–229.
72. Brinckmann J. (2005). Collagens at a glance. In: *Collagen*. Brinckmann J, Notbohm H, Müller PK, eds. Springer, Berlin, pp 1–6.
73. Egusa H, K Iida, M Kobayashi, TY Lin, M Zhu, PA Zuk, CJ Wang, DK Thakor, MH Hedrick and I Nishimura. (2007). Downregulation of extracellular matrix-related gene clusters during osteogenic differentiation of human bone marrow- and adipose tissue-derived stromal cells. Tissue Eng 13:2589–2600.
74. Sasaki J, TA Asoh, T Matsumoto, H Egusa, T Sohmura, E Alsberg, M Akashi and H Yatani. (2010). Fabrication of three-dimensional cell constructs using temperature-responsive hydrogel. Tissue Eng Part A 16:2497–2504.
75. Maherali N, R Sridharan, W Xie, J Utikal, S Eminli, K Arnold, M Stadtfeld, R Yachechko, J Tchieu, et al. (2007). Directly reprogrammed fibroblasts show global epigenetic remodeling and widespread tissue contribution. Cell Stem Cell 1:55–70.
76. Anguera MC, R Sadreyev, Z Zhang, A Szanto, B Payer, SD Sheridan, S Kwok, SJ Haggarty, M Sur, et al. (2012). Molecular signatures of human induced pluripotent stem cells highlight sex differences and cancer genes. Cell Stem Cell 11:75–90.

Address correspondence to:
Hiroshi Egusa, DDS, PhD
Division of Molecular and Regenerative Prosthodontics
Tohoku University Graduate School of Dentistry
4-1 Seiryo-machi, Aoba-ku
Sendai
Miyagi 980-8575
Japan

E-mail: egu@dent.tohoku.ac.jp

Received for publication July 26, 2013
Accepted after revision March 13, 2014
Prepublished on Liebert Instant Online March 13, 2014